REPORT

QUANTUM ENTANGLEMENT

# Spatial entanglement patterns and Einstein-Podolsky-Rosen steering in Bose-Einstein condensates

**Matteo Fadel, Tilman Zibold, Boris Décamps, Philipp Treutlein***

**Many-particle entanglement is a fundamental concept of quantum physics that still presents conceptual challenges. Although nonclassical states of atomic ensembles were used to enhance measurement precision in quantum metrology, the notion of entanglement in these systems was debated because the correlations among the indistinguishable atoms were witnessed by collective measurements only. Here, we use high-resolution imaging to directly measure the spin correlations between spatially separated parts of a spin-squeezed Bose-Einstein condensate. We observe entanglement that is strong enough for Einstein-Podolsky-Rosen steering: We can predict measurement outcomes for noncommuting observables in one spatial region on the basis of corresponding measurements in another region with an inferred uncertainty product below the Heisenberg uncertainty bound. This method could be exploited for entanglement-enhanced imaging of electromagnetic field distributions and quantum information tasks.**

Two quantum mechanical degrees of freedom are entangled (nonseparable) if the quantum state of one cannot be described independently of the other. When measurements are performed on both, entanglement results in correlations between the outcomes. Although entanglement can exist between any quantum degrees of freedom, the conflict with classical physics is particularly evident when the correlations are observed between measurement outcomes obtained in spatially separated regions. Einstein, Podolsky, and Rosen (EPR) pointed out (*1*) that if the correlations are sufficiently strong, local measurements in one region, *A*, can apparently change the quantum state in a spatially separated region, *B*, a scenario Schrödinger named "steering" (*2*). The possibility of steering between spatially separated systems implies that quantum theory is in conflict with a local realist description of the world (*3*, *4*). In fact, steering allows an observer in *A* to use her local measurement outcomes to predict the outcomes of noncommuting measurements in *B* with uncertainties below the Heisenberg uncertainty relation for B. EPR steering has been extensively explored with optical systems (*4*). Entanglement was observed between spatially separated atomic ensembles (*5*–*8*) and between individually addressable atoms in optical lattices (*9*, *10*), but EPR steering has not yet been achieved for more than two atoms (*11*). Demonstrating the EPR paradox with ensembles of massive particles is desirable, as it puts quantum physics to a stringent test in a regime of increasingly macroscopic systems (*4*). Moreover, it opens up perspectives for applications of such systems in quantum metrology and one-sided device-independent quantum information tasks, which exploit EPR steering as a resource (*12*).

Experiments with ultracold atomic ensembles recently made rapid progress, and a variety of nonclassical states can be prepared (*13*). Besides being of fundamental interest, such states find applications in quantum metrology (*14*), where the correlations between the constituent atoms are exploited to reduce the noise in atom interferometric measurements (*15*–*18*). Because of the large number of atoms involved, it is usually not possible to address and detect the atoms individually. In the case of Bose-Einstein condensates (BECs), it is even impossible in principle: The atoms are identical particles that occupy the same spatial mode. Still, quantum correlations between them can be characterized with the help of witness observables that involve only collective measurements on the entire ensemble (*19*, *20*). This approach has been used to reveal the presence of entanglement (*15*, *21*), EPR correlations (*22*), and even Bell correlations (*23*) in a cloud of atoms. However, these nonclassical correlations have not yet been observed directly by performing measurements on spatially separated subsystems. Moreover, several authors have questioned whether the concept of entanglement in systems of indistinguishable particles is fully legitimate and useful for tasks other than metrology [for a review see (*24*)].

Department of Physics and Swiss Nanoscience Institute, University of Basel, Klingelbergstrasse 82, 4056 Basel, Switzerland
*Corresponding author. Email: philipp.treutlein@unibas.ch

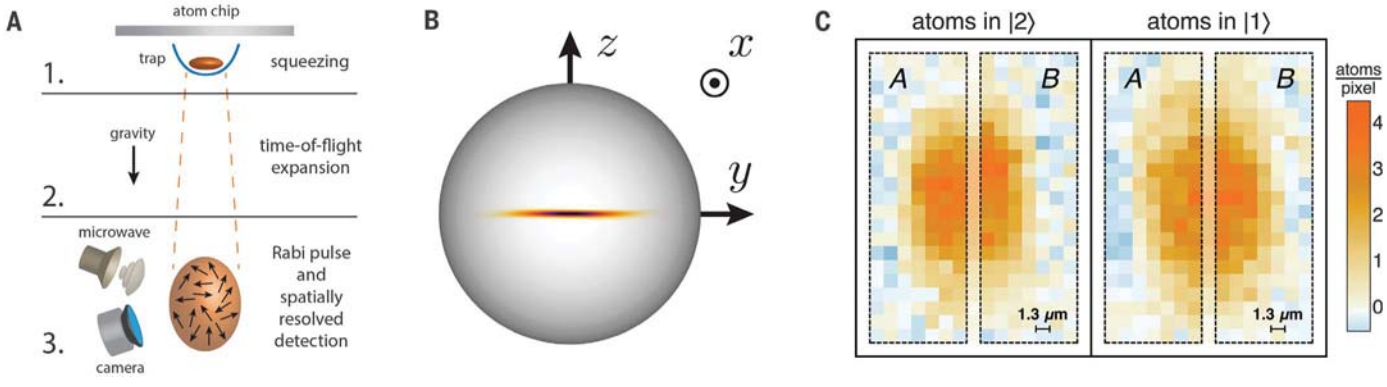


**Fig. 1. Extracting entanglement from spatially separated regions of a BEC.** (**A**) Experimental sequence. In step 1, we prepare a BEC in a spin-squeezed state on an atom chip. In step 2, the trapping potential is switched off and the BEC expands. In step 3, a Rabi rotation pulse is applied to select the spin component $\hat{S}_{\vec{n}}$ to be measured, followed by recording two high-resolution absorption images of the atomic density distributions in states $|1\rangle$ and $|2\rangle$. (**B**) Illustration of the spin-squeezed state on a sphere (Wigner function, representing the quantum fluctuations of the spin) and definition of the axes $\vec{n}$ used in the measurement of the entanglement and EPR steering criteria. (**C**) Single-shot absorption images of the atomic densities in $|2\rangle$ and $|1\rangle$, showing an example of regions *A* and *B* used to define the collective spins $\hat{S}^A$ and $\hat{S}^B$ entering in the entanglement and EPR steering criteria.

As pointed out in the theoretical work of (*24*), the presence of entanglement in an ensemble of indistinguishable particles can be unambiguously confirmed by extracting it into spatially separated modes, turning it into a resource for a variety of quantum information tasks. In our experiment, we demonstrate that entanglement can be extracted from spatially separated parts of a spin-squeezed BEC and use the entanglement to demonstrate the EPR paradox with an atomic system.

The quantum degrees of freedom in our experiment are two effective collective spins (*13*, *25*), $\hat{\vec{S}}^A$ and $\hat{\vec{S}}^B$, that describe the internal state of atoms in regions $A$ and $B$, respectively. Each atom is an effective two-level system with internal states $|1\rangle$ and $|2\rangle$. The component $\hat{S}_z^A = \frac{1}{2\eta_{\mathrm{eff}}^A}(\hat{N}_1^A - \hat{N}_2^A)$ is proportional to half the atom-number difference between the states, evaluated in region $A$. The normalization by $\eta_{\mathrm{eff}}^A$ (*25*) takes into account the finite resolution of the imaging system (*26*). A similar definition holds for $\hat{S}_z^B$. Other spin components can be measured by applying appropriate spin rotations before detection. To detect entanglement, we use the criterion from (*27*), where it was shown that for all separable states

$$\mathcal{E}_{\mathrm{Ent}} = \frac{4\,\mathrm{Var}\left(g_z\hat{S}_z^A + \hat{S}_z^B\right)\,\mathrm{Var}\left(g_y\hat{S}_y^A + \hat{S}_y^B\right)}{\left(\left|g_z g_y\right|\left|\left\langle\hat{S}_x^A\right\rangle\right| + \left|\left\langle\hat{S}_x^B\right\rangle\right|\right)^2} \geq 1 \qquad (1)$$

where $\mathrm{Var}(\cdot)$ denotes the variance and $g_z, g_y$ are real parameters that can be optimized to minimize $\mathcal{E}_{\mathrm{Ent}}$. Therefore, $\mathcal{E}_{\mathrm{Ent}} < 1$ is a sufficient condition to certify entanglement (nonseparability) between $A$ and $B$.

The variances in Eq. 1 quantify the uncertainty with which an observer in $A$ can predict (infer) the outcome of a spin measurement in $B$ on the basis of a corresponding measurement on her own system and are therefore called inferred variances. Because $\hat{S}_z$ and $\hat{S}_y$ do not commute, measuring both inferred variances requires repeated experiments on identically prepared systems. Correlations between $A$ and $B$ improve the prediction of $A$ for such noncommuting measurements performed by $B$ and decrease the product of inferred variances.

EPR steering is demonstrated if the correlations are so strong that the product of the inferred variances falls below the Heisenberg uncertainty bound for system $B$, i.e., there is a violation of the relation (*4*)

$$\mathcal{E}_{\mathrm{EPR}}^{A\to B} = \frac{4\,\mathrm{Var}\left(g_z\hat{S}_z^A + \hat{S}_z^B\right)\mathrm{Var}\left(g_y\hat{S}_y^A + \hat{S}_y^B\right)}{\left|\left\langle\hat{S}_x^B\right\rangle\right|^2} \geq 1 \qquad (2)$$

If there are no correlations between $A$ and $B$, the variances in Eq. 2 are minimized for $g_z = g_y = 0$, for which the spin uncertainty relation for $B$ is recovered. In the presence of a violation of Eq. 2, the observer $B$ must conclude that he is in the paradoxical situation considered by EPR, where the observer in $A$ can predict his measurement results without any classical communication. Note that a violation of Eq. 1 does not imply a violation of Eq. 2, whereas the converse is true. This reflects the fact that entanglement is necessary but not sufficient for EPR steering and that they are inequivalent types of correlations (*3*, *28*). Moreover, the asymmetry between $A$ and $B$ present in Eq. 2 implies that even if $A$ can steer $B$ (denoted $A\to B$), $B$ may not necessarily be able to steer $A$ ($B\to A$), as investigated both theoretically (*28*–*30*) and experimentally (*31*, *32*) in optics.

To demonstrate a violation of both Eqs. 1 and 2 with a massive many-particle system, we perform experiments with two-component BECs of $N = 590 \pm 30$ $^{87}$Rb atoms, magnetically trapped on an atom chip (*33*). The two components correspond to the hyperfine states $|F = 1, m_F = -1\rangle \equiv |1\rangle$ and $|F = 2, m_F = 1\rangle \equiv |2\rangle$ and occupy nearly identical spatial modes. They can be described by a collective spin $\hat{\vec{S}}$, referring to the entire BEC.

We prepare the BEC in a spin-squeezed state by controlling atomic collisions with a state-dependent potential, as described in (*18*, *21*, *23*). The spin-squeezed state features quantum correlations between the atoms, which reduce fluctuations of $\hat{S}_z$ and increase fluctuations of $\hat{S}_y$ while maintaining a large spin polarization in $\hat{S}_x$ (see Fig. 1B). We obtain typically −3.8(2) dB of spin squeezing according to the Wineland criterion (*34*). Alternatively, we can prepare the BEC in a coherent spin state, where the atomic internal states are uncorrelated.

To access spatially separated regions in the BEC, we use the sequence illustrated in Fig. 1A. After preparing the state, the atomic cloud is released from the trap and expands during a 2.2-ms time of flight. This expansion is nearly spin-independent (because collisional interactions are very similar for $|1\rangle$ and $|2\rangle$) and leads to a magnification of the atomic cloud. Next, we set the axis $\vec{n}$ of the spin components $\hat{S}_{\vec{n}}^A$ and $\hat{S}_{\vec{n}}^B$ to be measured by applying a Rabi rotation pulse to the entire atomic cloud. Immediately thereafter, we record two high-resolution absorption images (*35*) of the atomic density distributions in states $|2\rangle$ and $|1\rangle$ by illuminating the atomic cloud twice with a resonant laser beam. The imaging pulses project the spin state and

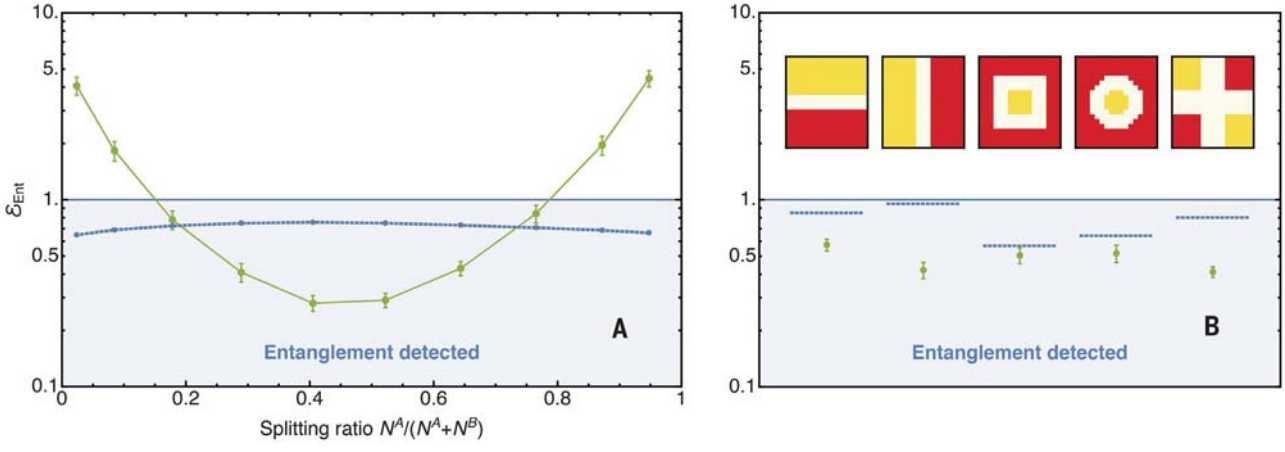


**Fig. 2. Spatial entanglement patterns in the atomic cloud.** (**A**) Entanglement criterion Eq. 1 evaluated for a spin-squeezed BEC (green points) for different horizontal positions of the one-pixel gap between regions $A$ and $B$ (see Fig. 1C), corresponding to different splitting ratios $N^A/(N^A + N^B)$. Lines are a guide to the eye, and error bars indicate 1 SEM. The blue points show the maximum violation (minimum value of $\varepsilon_{\mathrm{Ent}}$) that could be explained by detection cross-talk. (**B**) Entanglement between regions of different shapes ($A$ = yellow, $B$ = red) in a spin-squeezed BEC. The pixel pattern used for the analysis is illustrated above the respective data points, and the blue segments show the corresponding maximum violation expected by cross-talk.

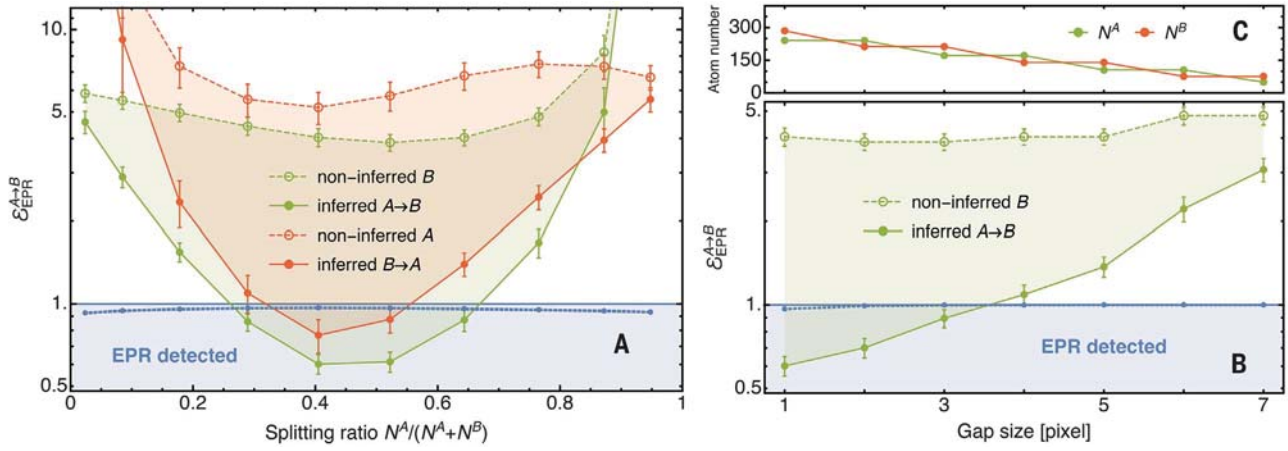


**Fig. 3. Observation of Einstein-Podolsky-Rosen steering.** (**A**) EPR steering criterion Eq. 2, evaluated for steering $A\to B$ (green filled circles) and $B\to A$ (red filled circles) in a spin-squeezed BEC, for different horizontal positions of the one-pixel gap (see Fig. 1C), corresponding to different splitting ratios $N^A/(N^A+N^B)$. EPR steering is strongest for intermediate splitting ratios. Empty circles: spin uncertainty relation involving the product of noninferred variances in region $B$ (green) and $A$ (red). Lines are a guide to the eye, and the shaded regions are the reduction of the uncertainty product in replacing the noninferred variances with the inferred ones. Blue points: maximum violation that could be explained by detection cross-talk. (**B**) EPR steering $A\to B$ for different widths of the gap in Fig. 1C. The center of the gap is fixed to the position showing maximum EPR steering in Fig. 3A. Even for increased gap size, we find a significant violation of the bound, confirming that the correlations cannot be explained by detection cross-talk between the regions. Lines and shaded regions as in (A). (**C**) Atom number in regions $A$ and $B$ as a function of the gap size.

simultaneously localize the atoms in well-defined positions. Figure 1C shows typical absorption images taken in this way. This experimental sequence is repeated thousands of times, alternating the measurement direction $\vec{n}$ along either $x$, $y$, or $z$.

We now define the two regions, $A$ and $B$, to be analyzed on all pairs of absorption images (Fig. 1C). Counting the atom numbers $N_1^A$ and $N_2^A$ in region $A$ realizes a single-shot projective measurement of the local spin $\hat{S}_{\vec{n}}^A = \frac{1}{2\eta_{\mathrm{eff}}^A}(\hat{N}_1^A - \hat{N}_2^A)$. The same approach is applied to region $B$, which yields $\hat{S}_{\vec{n}}^B$. The finite optical resolution and the motion of atoms during the imaging pulses amount to an uncertainty in the atomic position of 1.8 μm (2.5 μm) or 1.4 pixels (2.0 pixels) in the horizontal (vertical) direction. Consequently, spins near the boundary have only partial overlap with the region $A$ or $B$, which is taken into account by $\eta_{\mathrm{eff}}$ (*25*). Furthermore, spins overlapping with both $A$ and $B$ lead to detection cross-talk, which we reduce by leaving a gap of 1 pixel between the two regions. The experimentally determined spin variances include a contribution from detection noise, which can be independently measured and subtracted (*26*).

To detect entanglement between regions $A$ and $B$, we evaluate Eq. 1 for different positions of the gap, corresponding to different splitting ratios $N^A/(N^A+N^B)$, where $N^A = N_1^A + N_2^A$ and similar for $N^B$ (Fig. 2A, green dots). For a wide range of splitting ratios, we observe a violation of the inequality in Eq. 1 that goes far below the value that could be explained by detection cross-talk (*26*). This proves that the two local spins $\hat{S}^A$ and $\hat{S}^B$ are entangled. The extracted entanglement derives from the quantum correlations among the indistinguishable atoms in the initial state (*24*), as the expansion of the cloud, the spin rotation, and detection do not create such correlations.

An intriguing feature of our approach to extract entanglement (*24*) from a many-body state is that the subsystems can be defined a posteriori on the images. This is in contrast to other experiments where the subsystems are defined by the experimental setup (*5*–*8*) or by the source of the state (*4*, *31*). We exploit this feature to detect entanglement between regions $A$ and $B$ patterned in a variety of different shapes (Fig. 2B). That we observe entanglement between all such regions reflects the symmetry of the underlying many-body quantum state: The quantum state of the indistinguishable bosons in the condensate must be symmetric under particle exchange. Consequently, each atom is entangled with all other atoms, and the entanglement extends over the entire atomic cloud. In experiments with atoms in optical lattices, entanglement between different spatial bipartitions was observed by measuring entanglement entropy or concurrence, using systems of up to 10 atoms that were individually addressed (*9*, *10*). By comparison, our experiment reveals entanglement in ensembles of hundreds of atoms by using inequalities that apply in the continuous-variable limit.

The correlations in our system are strong enough to demonstrate an EPR paradox: Fig. 3A shows a measurement of the EPR criterion Eq. 2 for a horizontal splitting of the cloud and different positions of the gap. We observe EPR steering $A\to B$ (green data points) for intermediate splitting ratios. For comparison, we evaluate the spin uncertainty relation $4\,\mathrm{Var}(\hat{S}_z^B)\,\mathrm{Var}(\hat{S}_y^B)/|\langle\hat{S}_x^B\rangle|^2 \geq 1$ for system $B$, illustrating the reduction of the uncertainty product when replacing the noninferred variances with the inferred ones. As can be seen in Eq. 2, EPR steering is an asymmetric concept. By relabeling region $A$ as $B$ and vice versa, we can invert the roles of the steering and steered systems. This inverted scenario also shows EPR steering $B\to A$ (red data points in Fig. 3A). The asymmetry between the curves indicates the presence of technical noise in our system (*30*, *31*, *36*). For intermediate splitting ratios, we observe two-way steering $A\leftrightarrow B$, a prerequisite for observing the even stronger Bell correlations (*28*). We note that we also observe EPR steering if we do not subtract detection noise from the inferred variances [$\mathcal{E}_{\mathrm{EPR}}^{A\to B} = 0.73(6)$ for a splitting ratio of 0.4], and also for vertical instead of horizontal splitting of the cloud [$\mathcal{E}_{\mathrm{EPR}}^{A\to B} = 0.81(4)$ for a splitting ratio of 0.6].

Finally, we characterize the robustness of the observed EPR steering $A\to B$ to a variation of the gap size. We fix the central position of the gap such that the splitting ratio is 0.40 (the ratio maximizing steering $A\to B$ and $B\to A$ in Fig. 3A) and change the gap width symmetrically with respect to this position (Fig. 3C). We observe that EPR steering vanishes for large widths of the gap, where the size of the steered system is considerably reduced (Fig. 3B).

We have also performed measurements similar to those of Fig. 1 and Fig. 2 with the BEC initially prepared in a coherent spin state, showing no statistically significant violations of Eqs. 1 and 2 beyond detection cross-talk (*26*). The observed spin noise in each individual region $A$ or $B$ agrees well with projection noise of uncorrelated atoms, confirming our calibration of the imaging system.

Our method can be used for quantum metrology of electromagnetic field patterns. Consider an applied field that shifts the spin components $\hat{S}_y^B$ and $\hat{S}_z^B$ with respect to $\hat{S}_y^A$ and $\hat{S}_z^A$. The EPR entanglement allows one to detect this shift in

the $yz$ plane with an uncertainty characterized by the product of the inferred variances in Eq. 2. The EPR parameter $\mathcal{E}_{\mathrm{EPR}}^{A\to B} < 1$ quantifies by how much this measurement improves over the Heisenberg uncertainty bound for $\hat{S}^B$ and is thus a direct measure of the metrological enhancement provided by the EPR entanglement. Because our imaging method allows us to define the regions $A$ and $B$ a posteriori in a variety of shapes (Fig. 2), a single data set could be used to analyze dipole, quadrupole, and more complex patterns of the applied field. This is different from other field-sensing methods where the pattern is defined by the state preparation (*15*, *37*).

Beyond metrology, EPR steering is a resource for one-sided device-independent quantum information tasks (*12*). The asymmetry of the steering concept allows tasks such as quantum teleportation, entanglement swapping, or randomness certification to be performed in a situation where one of the involved parties can be trusted but not the other. An interesting perspective in this context is to distribute the correlations over macroscopic distances by splitting the atomic cloud with a double- or multiwell potential, exploiting the full control of BEC wave functions provided by the atom chip (*33*). Furthermore, our study raises the question of whether Bell correlations could also be observed between spatially separated regions. Although the EPR paradox can be demonstrated with Gaussian states and measurements and identical measurement settings in $A$ and $B$, a violation of a Bell inequality would require non-Gaussian states or measurements as well as the ability to measure different spin components in the two regions in a single run of the experiment (*38*). This could be achieved by rotating the collective spins $\hat{S}^A$ and $\hat{S}^B$ independently with on-chip microwave near-fields, followed by atomic fluorescence detection with single-atom resolution. In summary, our results open up a variety of perspectives for quantum science and technology with massive many-body systems.

Complementary to our work, spatially distributed multipartite entanglement was observed in (*39*) and entanglement of spatially separated modes was observed in (*40*).

## REFERENCES AND NOTES


1. A. Einstein, B. Podolsky, N. Rosen, *Phys. Rev.* **47**, 777–780 (1935).
2. E. Schrödinger, M. Born, *Proc. Camb. Philos. Soc.* **31**, 555 (1935).
3. H. M. Wiseman, S. J. Jones, A. C. Doherty, *Phys. Rev. Lett.* **98**, 140402 (2007).
4. M. D. Reid *et al.*, *Rev. Mod. Phys.* **81**, 1727–1751 (2009).
5. B. Julsgaard, A. Kozhekin, E. S. Polzik, *Nature* **413**, 400–403 (2001).
6. C. W. Chou *et al.*, *Nature* **438**, 828–832 (2005).
7. D. N. Matsukevich *et al.*, *Phys. Rev. Lett.* **96**, 030405 (2006).
8. J. Simon, H. Tanji, S. Ghosh, V. Vuletic, *Nat. Phys.* **3**, 765–769 (2007).
9. R. Islam *et al.*, *Nature* **528**, 77–83 (2015).
10. T. Fukuhara *et al.*, *Phys. Rev. Lett.* **115**, 035302 (2015).
11. E. Hagley *et al.*, *Phys. Rev. Lett.* **79**, 1–5 (1997).
12. D. Cavalcanti, P. Skrzypczyk, *Rep. Prog. Phys.* **80**, 024001 (2017).
13. L. Pezzé, A. Smerzi, M. K. Oberthaler, R. Schmied, P. Treutlein, arXiv:1609.01609 [quant-ph] (6 September 2016).
14. V. Giovannetti, S. Lloyd, L. Maccone, *Nat. Photonics* **5**, 222–229 (2011).
15. C. Gross, T. Zibold, E. Nicklas, J. Estève, M. K. Oberthaler, *Nature* **464**, 1165–1169 (2010).
16. A. Louchet-Chauvet *et al.*, *New J. Phys.* **12**, 065032 (2010).
17. I. D. Leroux, M. H. Schleier-Smith, V. Vuletić, *Phys. Rev. Lett.* **104**, 250801 (2010).
18. C. F. Ockeloen, R. Schmied, M. F. Riedel, P. Treutlein, *Phys. Rev. Lett.* **111**, 143001 (2013).
19. L. Amico, R. Fazio, A. Osterloh, V. Vedral, *Rev. Mod. Phys.* **80**, 517–576 (2008).
20. O. Gühne, G. Tóth, *Phys. Rep.* **474**, 1–75 (2009).
21. M. F. Riedel *et al.*, *Nature* **464**, 1170–1173 (2010).
22. J. Peise *et al.*, *Nat. Commun.* **6**, 8984 (2015).
23. R. Schmied *et al.*, *Science* **352**, 441–444 (2016).
24. N. Killoran, M. Cramer, M. B. Plenio, *Phys. Rev. Lett.* **112**, 150501 (2014).
25. J. Hu, W. Chen, Z. Vendeiro, H. Zhang, V. Vuletic, *Phys. Rev. A* **92**, 063816 (2015).
26. Supplementary materials are available online.
27. V. Giovannetti, S. Mancini, D. Vitali, P. Tombesi, *Phys. Rev. A* **67**, 022320 (2003).
28. M. T. Quintino *et al.*, *Phys. Rev. A* **92**, 032107 (2015).
29. S. L. W. Midgley, A. J. Ferris, M. K. Olsen, *Phys. Rev. A* **81**, 022101 (2010).
30. Q. Y. He, Q. H. Gong, M. D. Reid, *Phys. Rev. Lett.* **114**, 060402 (2015).
31. V. Händchen *et al.*, *Nat. Photonics* **6**, 596–599 (2012).
32. S. Wollmann, N. Walk, A. J. Bennet, H. M. Wiseman, G. J. Pryde, *Phys. Rev. Lett.* **116**, 160403 (2016).
33. P. Böhi *et al.*, *Nat. Phys.* **5**, 592–597 (2009).
34. D. J. Wineland, J. J. Bollinger, W. M. Itano, D. J. Heinzen, *Phys. Rev. A* **50**, 67–88 (1994).
35. W. Ketterle, D. S. Durfee, D. M. Stamper-Kurn, in *Proceedings of the International School of Physics "Enrico Fermi," Course CXL*, M. Inguscio, S. Stringari, C. E. Wieman, Eds. (IOS Press, Amsterdam, 1999), pp. 67–176.
36. K. Wagner *et al.*, *J. Phys. At. Mol. Opt. Phys.* **47**, 225502 (2014).
37. W. Muessel, H. Strobel, D. Linnemann, D. B. Hume, M. K. Oberthaler, *Phys. Rev. Lett.* **113**, 103004 (2014).
38. N. Brunner, D. Cavalcanti, S. Pironio, V. Scarani, S. Wehner, *Rev. Mod. Phys.* **86**, 419–478 (2014).
39. P. Kunkel *et al.*, *Science* **360**, 413–416 (2018).
40. K. Lange *et al.*, *Science* **360**, 416–418 (2018).


## ACKNOWLEDGMENTS

We thank M. D. Reid, P. D. Drummond, M. Oberthaler, T. Byrnes, and R. Schmied for useful discussions. **Funding:** This work was financially supported by the Swiss National Science Foundation. **Author contributions:** M.F., T.Z., and B.D. performed experiments and analyzed data, supervised by P.T. All authors discussed the results and contributed to the manuscript. **Competing interests:** The authors declare that they have no competing interests. **Data and materials availability:** All data needed to evaluate the conclusions in the paper are present in the paper and/or the supplementary materials.

## SUPPLEMENTARY MATERIALS

www.sciencemag.org/content/360/6387/409/suppl/DC1
Materials and Methods
Figs. S1 to S4
References (*41*–*43*)
Data File S1

28 June 2017; accepted 13 March 2018
10.1126/science.aao1850